Remote Quantification of the Trophic Status of Chinese Lakes

Sijia Li [a,b,c], Shiqi Xu[a], Kaishan Song[a], Tiit Kutser[c], Zhidan Wen[a*], Ge Liu[a], Yingxin Shang[a], Lili Lyu[a], Hui Tao[a], Xiang Wang[a], Lele Zhang[a], Fangfang Chen[a]

[a] *Northeast Institute of Geography and Agroecology, Chinese Academy of Sciences, Changchun 130102, China. P. R*

[b] *Key Laboratory of Space Ocean Remote Sensing and Application, Ministry of Natural Resources, National Satellite Ocean Application Service, Beijing 100081, China*

[c]*Estonian Marine Institute, University of Tartu, Mäealuse 14, 12618 Tallinn, Estonia*

Correspondence to: Zhidan Wen (wenzhidan@iga.ac.cn)

Abstract: Assessing eutrophication in lakes is of key importance, as this parameter constitutes a major aquatic ecosystem integrity indicator. The trophic state index (*TSI*), which is widely used to quantify eutrophication, is a universal paradigm in scientific literature. In this study, a methodological framework is proposed for quantifying and mapping *TSI* using the Sentinel Multispectral Imager sensor and fieldwork samples. The first step of the methodology involves the implementation of stepwise multiple regression analysis of the available *TSI* dataset to find some band ratios, such as blue/red, green/red, and red/red, which are sensitive to lake *TSI*. Trained with in situ measured *TSI* and match-up Sentinel images, we established the XGBoost of machine learning approaches to estimate *TSI*, with good agreement (R^2=0.87, slope=0.85) and fewer errors (MAE= 3.15 and RMSE=4.11). Additionally, we discussed the transferability and applications of XGBoost in three lake classifications: water quality, absorption contribution, and reflectance spectra types. We selected the XGBoost to map *TSI* in 2019-2020 with good quality Sentinel-2 Level-1C images embedded in ESA to examine the spatiotemporal variations of the lake trophic state. In a large-scale observation, 10-m *TSI* products from investigated 555 lakes in China facing

eutrophication and unbalanced spatial patterns associated with lake basin characteristics, climate, and anthropogenic activities. The methodological framework proposed herein could serve as a useful resource toward a continuous, long-term, and large-scale monitoring of lake aquatic ecosystems, supporting sustainable water resource management.

1 Introduction

Lakes, as valid sentinels of global or regional responses, are sensitive to anthropogenic activities and climate change (Mortsch et al., 1996; Quayle et al., 2002; Tranvik et al., 2009). The commonly used paradigm for studying eco-environmental monitoring and controlling of lakes is the status of eutrophication (Carlson, 1977). It is a combination of light, heat, hydrodynamics, and nutrients, such as nitrogen and phosphorus, which occurs through a series of biological, chemical, and physical processes of lakes (Guo et al., 2020). As a result of eutrophication, nutrient loading and productivity grow sharply, and even hypoxia and frequent outbreaks of harmful algal blooms are likely to produce toxins (Paerl et al., 2008, 2011). These processes can cause serious degradation of water quality and are detrimental to the ecosystem services functionality of lakes and reliable supply of drinking water (OECO, 1982). Once the eutrophication phenomenon becomes intense, ecological imbalances generally follow (Smith et al., 2006). Hence, knowledge of eutrophication process can provide us with an understanding of the structure and function of lake ecosystems that give rise to environmental changes. We can then predict future trends and develop appropriate mitigation strategies.

Several lakes experience eutrophication processes because of excessive nutrient enrichment (Lund, 1967; Smith et al., 1999; Wetzel, 2001). At the global scale, 63.1% of lakes larger than 25 km^2 are eutrophic and 54% of Asian lakes (Wang et al., 2018), as well as 53% of European lakes (ILEC et al., 1994). Lake eutrophication has become a global water quality issue affecting most freshwater ecosystems (Matthews, 2014). Currently, many pollutions control measures and management strategies have been implemented that are specific to individual lakes or to lakes, in general (USEPA, 2002). However, there is still insufficient information to address lake eutrophication related to environmental disturbances or changes. Realization of lake eutrophication has been a serious situation for some lakes; therefore, we provided some reasons to suggest the need for large-scale research. First, different environmental factors control the trophic status of lakes at local and multiple scales (e.g., Wiley et al., 1997). Specifically, biotic factors may dominate the eutrophic state of individual lakes, and we can understand the mechanism processes by lake-specific sampling. In contrast, abiotic factors and their linkages are pivotal factors that determine lake biogeochemistry at multiple scales (Sass et al., 2007). It is often necessary to study a number of lakes with different characteristics and catchments to understand the mechanisms of spatio-temporal patterns. Therefore, an up-scaling study of trophic status is required to understand the evolution prospects of lakes in response to changes in global and regional environments. Second, multi-year environmental and climatic conditions require long-term field studies and observations to understand the temporal pattern in important trophic status processes. In addition, relatively large datasets are needed considering the spatial extent because environmental factors are integrated to determine the trophic status of lakes. It can promote data organization and enable us to address an emergency and establish scientific measures for water resource management (Cunha et al., 2013; Smith and Schindler, 2009). Thus, eutrophication should be rapidly assessed using easy-to-analyze indices and enforcement methods for large-scale and high-frequency applications.

Evaluating the trophic state of lakes has been an important topic for decades

(Carlson, 1977; Smith and Schindler 2009). The traditional method uses chlorophyll-a, transparency, nutrients, and other variables as water quality indicators by field in situ sampling and laboratory measurements (Rodhe, 1969). Subsequently, Carlson (1977) introduced a numerical *TSI* that should have replaced descriptive values like “oligotrophic,” “mesotrophic,” or “eutrophic”. The replacement has not occurred, but the *TSI* proposed by Carlson is a common method to determine the trophic state level of aquatic environments (Aizaki et al., 1981). The traditional method for calculating *TSI* is based on collected in situ data. The sampling itself and subsequent laboratory measurements are labor-intensive and expensive, often also logistically difficult to perform. This limits our capability to monitor hundreds or thousands of lakes for eutrophication, not speaking about the majority of 117 million of lakes on Earth (Verpoorter et al. 2014). Moreover, the TSI calculated for one or a few discrete samples do not represent spatial distribution of TSI within (especially larger) lakes. This could limit the large-scale assessment of eutrophication as well as the understanding of biogeochemical cycles.

Satellite remote sensing is a useful tool for monitoring inland waters (Palmer et al 2015). Ocean water-color sensors, such as Medium Resolution Imaging Spectrometer (MERIS) or Ocean and Land Colour Instrument (OLCI) have too low spatial resolution (300 m) for majority of lakes on Earth. Land remote sensing seosor like Landsat Operational Land Imager (OLI), Sentinel-2 Multispectral Imager (MSI; 10-60 m) and Satellite pour l'Observation de la Terre (SPOT) with high spatial resolution (5–30 m) are not designed for water remote sensing (lack critical spectral bands, SNR is not sufficient for water, etc.). Compared to OLI and SPOT sensors, MSI has a more adequate radiometric resolution (12-bits) and 13 spectral bands, including four visible and SWIR channels (Drusch et al., 2012). Inland water TSI has been produced for large lakes using

MODIS sensor (Wang et al 2018). However, this study is for more than 2000 large lakes (due to the spatial resolution of the sensor). The Copernicus Land Monitoring Service has started to produce TSI for lakes large enough to be mapped with 100 m pixel size using Sentinel-2 MSI. However, this product is available only for Europe and some parts of Africa.

Instead of individual parameters, several studies (e.g., Morel and Prieur, 1977; Gurlin et al., 2011; Huang et al., 2014; Sass et al., 2007; Thiemann & Kaufmann, 2000; Yin et al. 2018) have also provided empirical relationships expressed as band combinations or baseline methods to acquire Chl-a, Secchi or nutrients related to potential *TSI* calculations in regional lakes. However, the accuracy of these empirical relationships for transferring knowledge from some representative lakes to large-scale lake groups is limited by large uncertainties (i.e., in areas with different water quality concentrations and atmospheric component influences, fewer lakes can be used with more heterogeneous influences and uniform algorithms) (Oliver et al., 2017). Considering the requirement of a uniform and universal relationship to quantify the trophic status of lakes, an alternative method using high-frequency and spatial resolution of the sensor is a significant challenge. Recently, technological developments, such as machine learning algorithms, have allowed the usage of remotely sensed imagery to successfully investigate water quality parameters using artificial intelligence (Reichstein et al., 2019; Pahlevan et al., 2020; Cao et al., 2020). The potential application and development of machine learning for remote quantification of water quality is attributed to the following advantages: requirement of little prior knowledge, rich features can be captured, and robust relationships can be obtained. These processes avoid bias and uncertainty from the regional environmental background as well as complications due to atmospheric components of traditional remote sensing-derived relationships over large-scale, i.e. for multiple lakes. Given the novel application of remote sensing and machine learning, this is a gap to fill for large-scale research of monitoring trophic states.

Environmental issues fueled by rapid economic growth in China have significantly increased in the last three decades. Lake eutrophication is a serious issue, with large variability in terms of trophic status and optical properties. However, most studies (Jin, 2003, 2005; Fragoso et al., 2011; Huang et al., 2014) have addressed eutrophication concerns in only a single lake or two lakes since the 1990s. It is acknowledged that a rapidly growing economy and anthropogenic activities (e.g., elevated nutrient loading and increasing air pollution) accelerate the aging process of lakes (Wu et al., 2011; Shi et al., 2020). Therefore, it is critical to objectively assess the trophic status and pay attention to protect the aquatic environment. We aim to provide a robust machine learning algorithm and remote sensing flowchart from simultaneously retrieved *TSI* over a wide range of bio-optical compositions in different lakes. The objectives of our study were to: (1) examine biogeochemical parameters and assess trophic status, (2) calibrate and validate the *TSI* model using different machining learning algorithms from MSI-imagery derived remote sensing reflectance spectra (*Rrs*), with different lake classifications; and (3) quantify and map the trophic status of typical 555 lakes in five Chinese limnetic regions.

2 Materials and methods

2.1 *Study area and sampling process*

China is located in the east of Asia with a land area of 9,600,000 square kilometers and a population of over 1.4 billion. The terrain of China descends from west to east in three steps. Due to a vast territory span, this country has diverse climatic, geographical, and geological conditions. There are 2,693 natural lakes (with area >1.0 km^2) that are distributed in China (Ma et al., 2011). Protection and sustainable management of these lakes have been priorities, considering the degradation of water quality over several decades. In this study, a total of 45 lakes were visited and 431 samples were collected in early April 2016 to late October 2019 (Table S1 and Fig. 1), which was the highest productive season, as identified by Carlson's *TSI* model. These datasets were analyzed and published in (Li et al., 2021; Song &Li et al., 2019; Song et al., 2020). Our lake dataset was collected from various types of lakes across China, and efforts were made to examine lake trophic status from a wide range of water quality parameters, lake sizes (0.5 to 4, 256 km^2), lake elevation (10 to 4, 525 m), and climatic zones (Song &Li et al., 2019). In the field, some small-size lakes were sampled in the middle, and signal sample was used to represent the water qualities, while others were sampled at multiple locations evenly distributed over the lake. The water samples were collected approximately 0.5 m below the surface, and then stored in 1 L amber HDPE bottles and kept in a portable refrigerator (4 ℃) before being transported to the laboratory. During the sampling process, the Secchi disk depth (SDD, m) was measured using a black-and-white Secchi disk. The pH and electrical conductivity (EC, $\mu s\ cm^{-1}$) were recorded using a portable multi-parameter water quality analyzer (YSI 6600, 170 U.S).

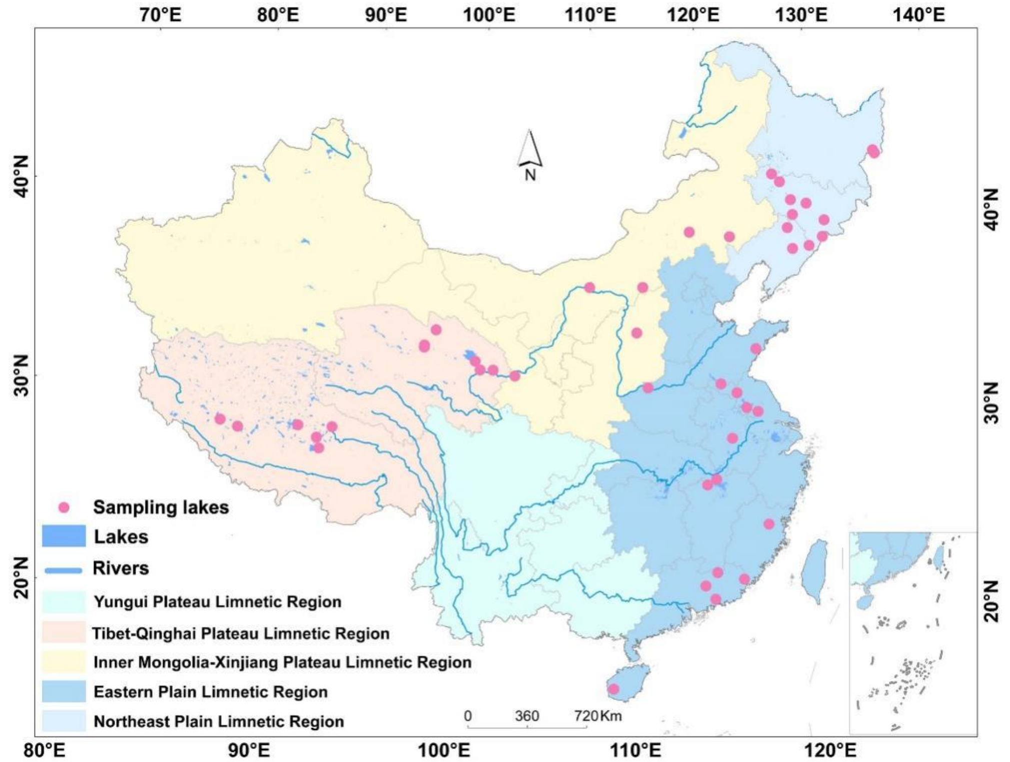

Figure 1：**Location of lake sites.**

2.2 Laboratory analysis

A transferred portion of each bulk water sample was immediately filtered with 0.45-μm pore size Whatman cellulose acetate membrane filters in the laboratory. It is to be noted that some remote Tibet and Qinghai lake samples had to be filtered during fieldwork. Chlorophyll-a (Chl-a) was extracted from the filters using a 90 % buffered acetone solution at 4° C under 24 h dark conditions. According to the SCOR-UNESCO equations (Jeffrey and Humphrey, 1975), the concentration of Chl-a (μg L^{-1}) was determined using a UV-2600PC spectrophotometer at 750 nm, 663 nm, 645 nm, and 630 nm. Dissolved organic carbon (mg L^{-1}) concentrations were determined using a total organic carbon analyzer. Total nitrogen (TN) and total phosphorus (TP) concentrations (mg L^{-1}) were measured using a continuous flow analyzer (SKALAR, San Plus System, the Netherlands) using a standard procedure (APHA/AWWA/WEF, 1998). In addition, total suspended matter (TSM, mg L^{-1}) concentrations were obtained gravimetrically using pre-combusted 0.7-μm pore size Whatman GF/F filters. All preprocesses (e.g., filtration and concentration quantification) of all water samples were undertaken within two days in the laboratory. The procedures are provided in detail in Li et al. (2021).

The bulk samples were again filtered through a 0.7-µm pore size glass fiber membrane (Whatman, GF/F 1825-047) to retain particulate matter. The water from particulate matter measurements was then filtered through a 0.22-µm pore size polycarbonate membrane (Whatman, 110606) in order to measure chromophoric dissolved organic matter (CDOM) absorption of each sample. According to the quantitative membrane filter technique (Cleveland and Weidemann, 1993), the light absorption of total particulate matter $a_p(\lambda)$ can be separated into phytoplankton pigment absorption $a_{ph}(\lambda)$, non-algal particles $a_d(\lambda)$, and CDOM absorption $a_{CDOM}(\lambda)$. The optical density (OD) of the particulate matter retained in the filters was measured using a UV-2600PC spectrophotometer at 380–800 nm, with a blank membrane as a reference at 380–800 nm. The filters were then bleached using a sodium hypochlorite solution to remove phytoplankton pigment and measured again using a spectrophotometer. Finally, the phytoplankton pigment absorption $a_{ph}(\lambda)$ was calculated by subtracting $a_d(\lambda)$ from the total particulate matter $a_p(\lambda)$. The absorption coefficients of the optical active substance (OACs) were calculated according to Song et al. (2013).

2.3 Trophic status assessment of lakes

Several studies have proposed different indices of the lake trophic state (Aizaki et al., 1981; Carlson, 1977). Carlson's trophic state index used five variables, such as Chl-a, TP, TN, SDD, and chemical oxygen demand (COD), to characterize the trophic state. However, there are no optical characteristics for TN, TP and COD to manifest in changes of remote sensing reflectance, which may bring more uncertainties or errors. Thus, Chl-a, TP, and SDD were selected to assess the trophic status according to the modified Carlson's trophic state index (*TSI*). The *TSI* can be calculated using individual TSI_M(Chl-a), TSI_M(SDD), and TSI_M(TP) using the following equations:

$$TSI_M(Chl\text{-}a) = 10 \times \left(2.46 + \frac{\ln Chl - a}{\ln 2.5}\right) \tag{1}$$

$$TSI_M(SDD) = 10 \times (2.46 + \frac{3.69 - 1.52 \times \ln SDD}{\ln 2.5}) \tag{2}$$

$$TSI_M(TP) = 10 \times (2.46 + \frac{6.71 + 1.15 \times \ln(TP)}{\ln 2.5}) \tag{3}$$

$$TSI = 0.54 \times TSI_M(Chl\text{-}a) + 0.297 \times TSI_M(SDD) + 0.163 \times TSI_M(TP) \tag{4}$$

Where, the *TSI* below 30 correspond to oligotrophic waters, above 50 are eutrophic and *TSI* between 30 and 50 in mesotrophic (Carlson, 1977).

2.4 Muti-Spectral Instrument imagery and atmospheric correction

Sentinel-2A/B MSI imagery was acquired from the Copernicus Open Access Hub of the European Space Agency. Altogether, 210 scenes of cloud-free Level-1C images covering the lakes were downloaded with a time window of ±7 days from in situ measurements. The Case 2 Regional Coast Color processor (C2RCC) was used to remove atmospheric effects. An average of 3×3-pixels centered at each in situ sampling station was used in the further analysis. All the processes were performed using the Sentinel Application Platform (SNAP) version 7.0.0. A flowchart of the process is shown in Fig. 2.

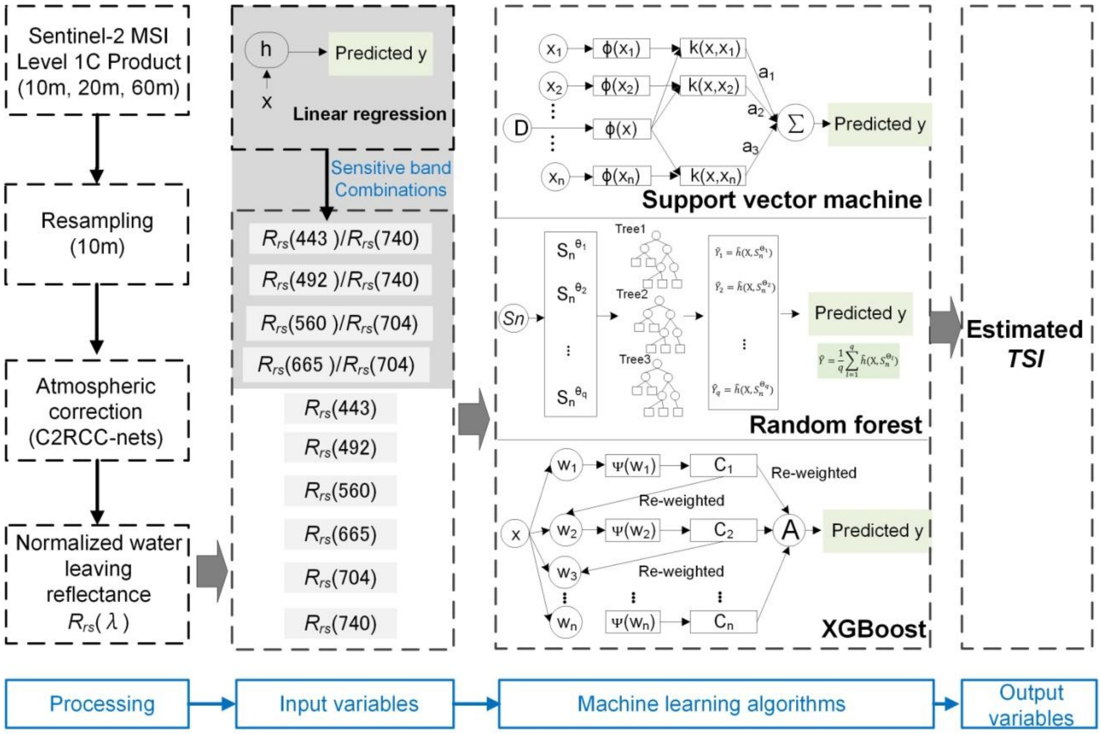

Figure 2 ： Workflow of the Sentinel-2 MSI data and machine learning algorithms for estimating *TSI*

2.5 Machine learning algorithms

As a branch of artificial intelligence, the application of machine learning is growing in the field. Machine learning can automatically analyze huge chunks of data, develop optimal models, generalize algorithms, and make predictions. These approaches have been applied in a variety of eco-environmental and remote sensing fields (Mountrakis et al., 2011; Pahlevan et al., 2019). Hence, we employed four representative machine learning algorithms, namely linear regression (LR), support vector machine (SVM), XGBoost (XGB), and random forest (RF) (Supplementary data, methods), to establish a *TSI* model. To strengthen the robustness, band combinations sensitive to *TSI* were determined by LR (Fig. 2), and were added to the procedure of machine learning algorithms as input variables. Subsequently, the output variable was the predicted *TSI*. The in situ measured samples were then randomly divided into a calibration dataset (70%, 287 lake samples) and validation dataset (30%, 144 lake samples) using MATLAB software. The *TSI* modeling procedure considering machine learning and Multiple Linear Regression (MLR) was processed using the R software.

2.6 Classifications of lakes

In order to provide further feasibility for the application and availability of the *TSI* model, the in situ measured samples were classified in three ways (Fig. 3):

a) based on water quality: Salinity classification referred to the threshold value of electrical conductivity (named EC, EC=1000 $\mu S\ cm^{-1}$) (Duarte et al., 2008), following which the lakes were divided into brackish lakes (*N*=100 samples) and fresh water lakes (*N*=331 samples). Dissolved organic carbon (DOC) in global lake water classification referred to the volume weighted averaged DOC level of global lakes (3.88 mg L^{-1}) according to Toming et al., (2020), following which lakes were divided into high DOC lake (*N*=224 samples) and low DOC lake (*N*=207 samples).

b) based on optical absorption contribution: Optical absorption classification referred to Prieur and Sathyendranath (1981), where the total light absorption of water can be separated from phytoplankton pigment absorption, non-algal particles, and CDOM absorption, respectively. The relative percentage of absorption contribution of OACs can be divided into phytoplankton-type (Phy-type) lakes (*N*=54 samples), non-algal particles-type (NAP-type) lakes (*N*=109 samples), CDOM-type lakes (*N*=177 samples), and mix-type lakes (*N*=91 samples).

c) based on reflectance spectra: In order to discern the different optical characteristics of lakes, the derived MSI reflectance was clustered using the k-means clustering approach with a gap statistic (Neil et al., 2018). We identified 431 MSI reflectance *Rrs*(λ) spectra for three branches (Table S3), and the *Rrs*(λ) spectra are shown in Fig.3.

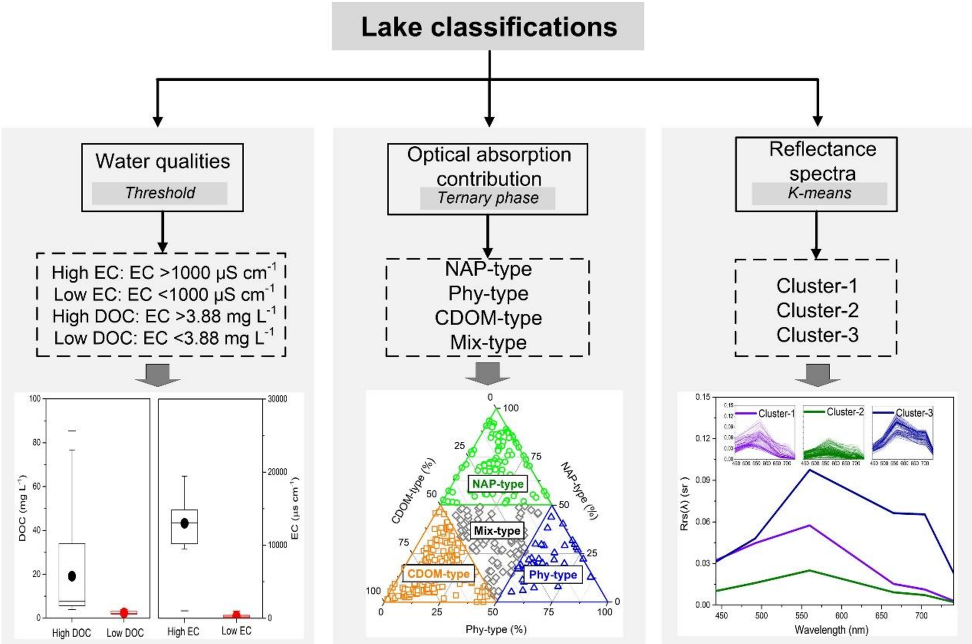

Figure 3: Lake classifications considering three ways, i.e., water quality, optical absorption contribution and reflectance spectra. ANOVA analysis was conducted in different classifications (p<0.001) (Table S3).

2.7 Statistical analyses and accuracy assessment

Statistical analysis, including descriptive statistics, correlation (r), regression (R^2), and ANOVA analyses, were implemented with Statistical Program for Social Science software (version 16.0; SPSS, Chicago, IL, USA). Correlation and regression analyses were used to examine the relationships between the water quality parameters and absorption coefficients of OACs as well as the *TSI* model calibration and validation. The differences in trophic status, EC classification, DOC classification, absorption coefficients of OAC classification, and MSI reflectance spectra classification for *TSI* model validation were assessed using one-way ANOVA. The significance level was set at $p<0.05^*$. The mean normalized error (MAE) and root mean square error (RMSE) were used to assess the performance of the *TSI* model (Supplementary data, accuracy assessment).

3 Results

3.1 Aquatic environmental scenery

The water qualities and bio-optical properties of our samples covered a wide range, revealing different geographical environmental scenery (Tables S1 and S2-4). The EC and DOC concentration showed high variability, ranging for example, from 3345.31 μs cm^{-1} (TuoSu, TS20) in Tibet-Qinghai region to 0.17 μs cm^{-1} (Qingnian, QN2) in Northeast region. For the water quality parameters to characterize *TSI*, the Chl-a concentration ranged from 0.12 to 100.22 μg L^{-1}, with the highest value recorded in TaiPingChi (TPC5) and the lowest value in NamoCo (NMC36). The range of TP was from 0.003 mg L^{-1} (Erlong, EL8) to 2.17 mg L^{-1} (Dali, DL7), and SDD ranged from 0.17 m (Chalhu, CH32) to 9.47 m (NMC36) for surveyed lakes, respectively. Overall, the maximum values of EC, DOC, turbidity, Chl-a, TSM, and SDD were 196782.35, 948.4, 723.3, 770.92, 614.58, and 55.71 fold greater than the minimum values, respectively, indicating that our dataset was representative of diverse water qualities.

Lake samples were grouped into different classifications based on water quality (e.g., EC and DOC), optical absorption contribution, and reflectance spectra (Table 1 and Fig. 3). The results indicated that all water qualities showed significant differences ($p<0.05$) under different lake classifications. For example, brackish lakes showed higher average values of SDD, TP, DOC, and optical attributions of OAC values than those of fresh water lakes, but the turbidity, Chl-a, and TSM concentrations were lower. Lakes equipped with low DOC levels had a low average value of SDD than that of lakes with high DOC levels. NAP-type lakes exhibited the highest average Chl-a and DOC values, whereas Phy-type lakes had the highest average turbidity and TSM values, and the highest average SDD and TP values were recorded in CDOM-type and Mix-type lakes, respectively. For reflectance spectra classifications (Fig. 3), the highest average EC, SDD, and DOC were recorded in cluster-1 lakes, the highest average turbidity and TP was shown in cluster-3 lakes and the highest average TSM was found in cluster-2 lakes.

Table1 (a) Averaged values (Avg.) of water quality and bio-optical properties considering lake classifications and (b) ANOVA analysis (*F* value) among them

cations	*N*	EC	Turbidity	SDD	Chl-a	TP	DOC	TSM	a_{ph}(440
Brackish	100	12986.28	8.83	2.21	4.18	0.45	33.31	8.42	0.23
Fresh	331	302.39	21.75	1.43	8.58	0.07	4.28	19.52	0.56
High DOC	224	5988.93	23.90	1.39	10.42	0.25	19.07	21.50	0.68
Low DOC	207	276.19	12.45	1.85	4.46	0.06	2.29	11.98	0.27
NAP-type	54	5156.02	11.28	1.58	14.26	0.09	18.75	15.99	1.29
Phy-type	109	825.48	43.28	0.65	6.85	0.10	4.75	37.18	0.46
CDOM-type	177	4081.96	4.44	2.43	3.64	0.13	9.70	4.99	0.13
Mix-type	91	3424.07	19.40	1.17	12.05	0.34	16.48	16.22	0.70
Cluster-1	87	6948.28	4.46	2.38	2.64	0.08	17.92	5.76	0.26
Cluster-2	215	2728.71	6.18	2.05	8.57	0.07	7.18	5.81	0.35
Cluster-3	129	1626.05	46.68	0.36	9.19	0.37	12.73	42.59	0.84
Brackish	100	-	18.7**	21.8**	12.0**	68.9**	486.5**	20.4**	16.6**
Fresh	331								
High DOC	224	93.8**	19.8**	10.0**	32.2**	23.3**	-	21.0**	38.0**
Low DOC	207								
NAP-type	54	7.4**	71.6**	46.0**	21.0**	7.1**	13.5**	73.0**	-
Phy-type	109								
CDOM-type	177								
Mix-type	91								
Cluster-1	87	220.9**	17.9**	25.2**	312.7**	11.0**	18.5**	18.9**	26.1**
Cluster-2	215								
Cluster-3	129								

The unit of TN, TP, DOC and TSM is mg L^{-1}; EC is μs cm^{-1}; Chl-a is μg L^{-1}; turbidity is NTU (nephelometric turbidity unit). Significance levels are reported as significant (noted with *, 0.05>*p*>0.01) or highly significant (noted with **, *p*<0.01).

3.2 Trophic status assessment

The trophic status of 45 lakes across China, from where in situ samples were collected, was evaluated (Fig. 4a). Our results showed that there were 13 oligotrophic (3.02 %), 199 mesotrophic (46.17 %), and 219 eutrophic (50.81 %) samples. Because our samples were collected in different seasons and eutrophication is time-dependent, the *TSI* values of samples within a lake were averaged. It can be shown that only five lakes accounting for 11.1% of investigated lakes were characterized with an oligotrophic status, 17 lakes accounting for 37.8 % were mesotrophic, and 23 lakes accounting for 51.1 % were characterized with eutrophic status. These eutrophic lakes were distributed in the eastern region of China (Fig. 4b), and were associated with a highly concentrated human population and economic development. Moreover, the ANOVA results showed that the *TSI* of lake samples were significantly different considering lake classifications (Fig. 4c, and d).

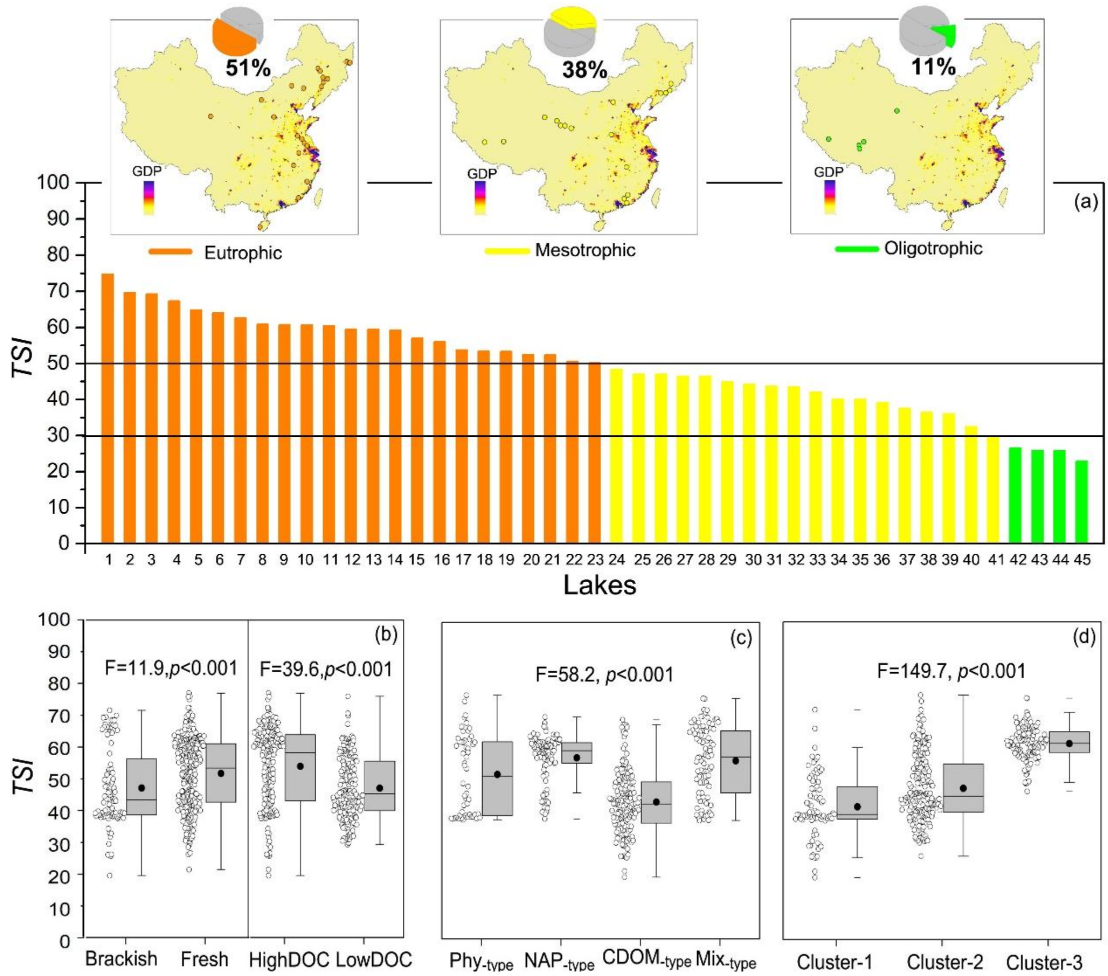

Figure 4: (a) is the averaged *TSI* in collected samples from lakes across China and their spatial distribution. The number of lakes can be found in TableS1. The box plots of *TSI* at different classifications of water quality (b), optical absorption contribution types (c) and reflectance spectra (d). The balls beside the boxes are the lake samples, and the black balls in the boxes represent the mean values. The horizontal edges of the boxes denote the 25th and 75th percentiles; the whiskers denote the 10th and 90th percentiles.

3.3 Calibration and validation of *TSI* model

In this section, multiple linear regression was used to identify significantly sensitive spectral variables related to *TSI* (Table 2 and Fig. 2). Of the band combinations validated in the study (*N*=144), the blue/red [*Rrs*(443)/*Rrs*(740), *Rrs*(492)/*Rrs*(740)], and green/red [*Rrs*(560)/*Rrs*(704), *Rrs*(665)/*Rrs*(704)] band ratios showed a good regression coefficient (R^2>0.59) with *TSI* (Table S5). These band combinations provided certain sensitive spectral variables that responded to the lake eutrophic status. Hence, to strengthen the robustness of the three machine learning models, the blue/red and green/red combinations above were considered as the input variables as well as six spectral variables (*Rrs*(λ) at 443, 492, 560, 665, 709, and 740 nm). Likewise, the output variables were estimated using *TSI* to examine the performances (Fig. 5). The results showed that when XGBoost was applied to the validation data (*N*=144), the performance of the model was excellent (R^2=0.87, slope=0.85) with low errors (MAE= 3.15, RMSE=4.11). The support vector machine (R^2=0.71, slope=0.77, MAE=4.67, RMSE=6.11) and random forest (R^2=0.85, slope=0.84, MAE=3.31, RMSE=4.34) models also showed significant performance. These results demonstrate the potential of using XGBoost by considering band combinations to derive *TSI* from Sentinel products.

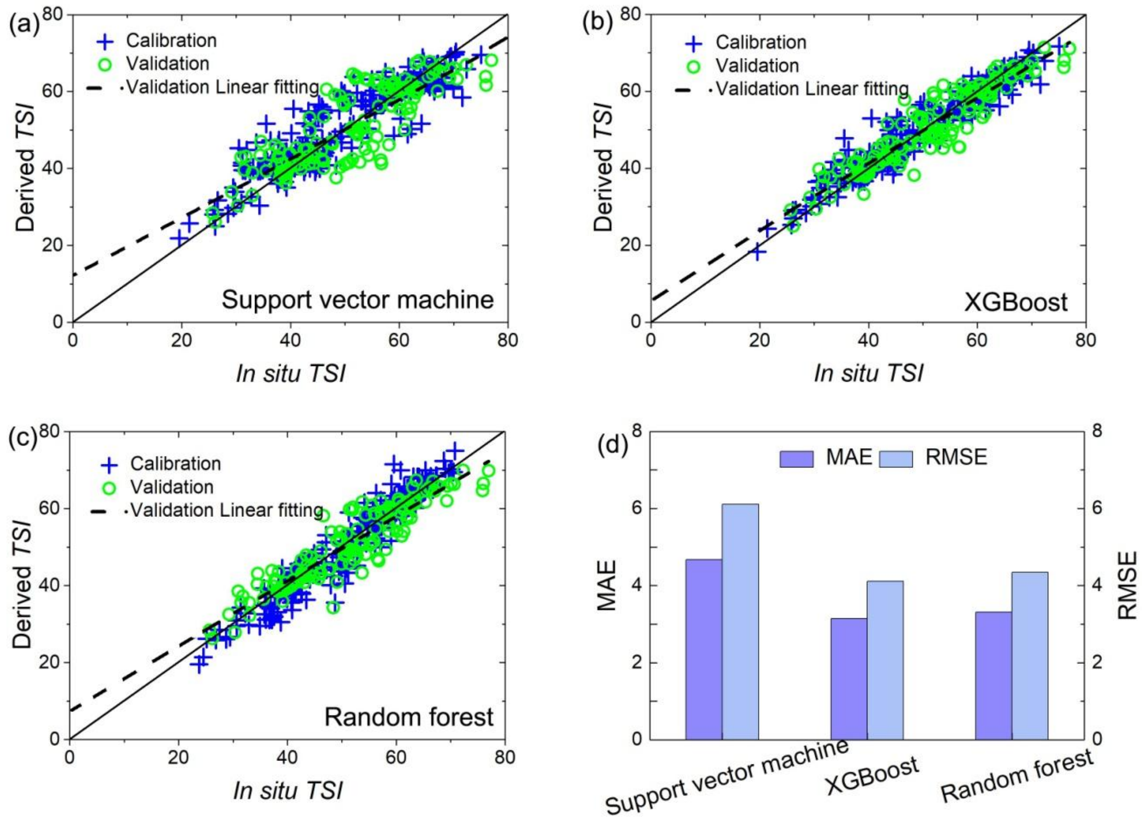

Figure 5: Relationships between in situ and derived *TSI* for both model training and testing samples by support vector machine (a), XGBoost (b) and random forest (c), as well as their errors (d).

Table 2 Multiple linear regression between measured- and estimated- *TSI* from the MSI spectral bands after using C2RCC processor

Band combinations	Datasets	*N*	Fitting equation	R^2	Errors	Plots figures
Band 1/ Band 6 (Blue/Red)	Calibration	287	TSI = -8.51ln [Rrs(B1)/Rrs(B6)] + 63.47	0.76	MAE = 6.45 RMSE = 5.85	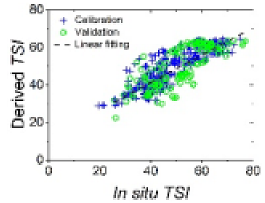
	Validation	144	$TSI_{derived}$= 0.73×$TSI_{in\ situ}$+ 11.868	0.61	MAE = 6.26 RMSE =7.48	
Band 2/ Band 6 (Blue/Red)	Calibration	287	TSI = -8.87ln [Rrs(B2)/Rrs(B6)] + 67.91	0.77	MAE = 4.57 RMSE = 5.74	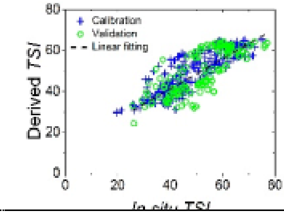
	Validation	144	$TSI_{derived}$ = 0.74×$TSI_{in\ situ}$ + 11.751	0.60	MAE = 6.32 RMSE =7.57	
Band 3/ Band 5 (Green/Red)	Calibration	287	TSI = -13.63ln [Rrs(B3)/Rrs(B5)] + 67.26	0.77	MAE = 4.55 RMSE = 5.70	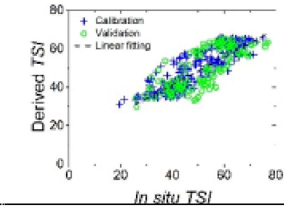
	Validation	144	$TSI_{derived}$ = $0.72 \times TSI_{in\ situ} + 12.44$	0.59	MAE = 6.39 RMSE = 7.66	
Band 4, Band 5 (Red/Red)	Calibration	287	TSI = -44.15×[Rrs(B4)/Rrs(B5)] + 108	0.80	MAE = 4.39 RMSE = 5.43	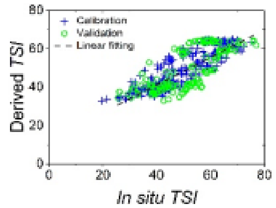
	Validation	144	$TSI_{derived}$ = $0.72 \times TSI_{in\ situ} + 12.32$	0.59	MAE = 6.85 RMSE = 7.94	

3.4 *TSI* model application to lake classifications

The *TSI* model calculated by XGBoost was assessed by comparing derived and in situ *TSI* considering different lake classifications (Fig. 6). We aimed to provide a universal *TSI* model and evaluate its feasibility in different aquatic environments. Significant agreement (slope>0.91, R^2>0.91) between derived and in situ *TSI* was observed in lakes with high DOC levels (DOC>3.88 mg L^{-1}) and EC values (EC>1000 μS cm^{-1}), with low errors. For lakes classified by different absorption contributions, the NAP-type (slope=0.98, R^2=0.88) and Phy-type (slope=0.82, R^2=0.92) samples generally showed a positive derived performance than those of Phy-type, CDOM-type, and Mix-type, respectively. In addition, a significant relationship between derived and in situ *TSI* can be described for lakes with cluster-1 reflectance spectra, with slope=0.91, R^2=0.87, RMSE=2.87, and MAE=2.29.

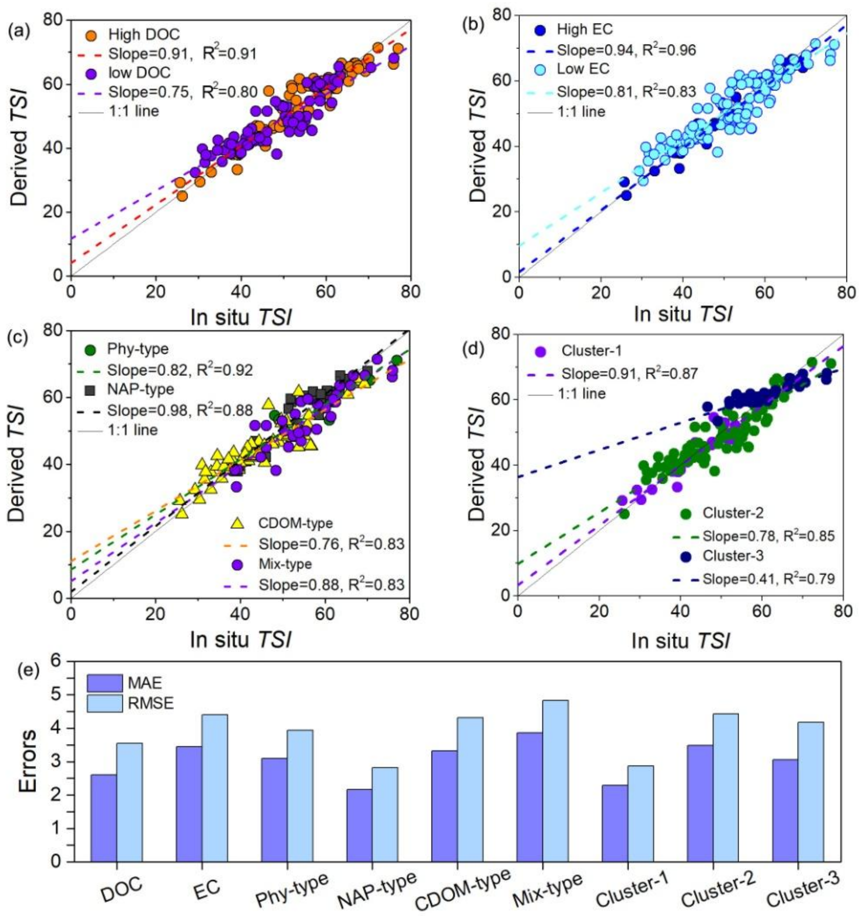

Figure 6: Scatter plots of derived- and in situ- *TSI* by XGBoost for validation samples (*N*=144) according to lake classifications, such as water quality (DOC and

EC) (a-b), absorption contribution (c), reflectance spectra(d) with the 1:1 line (red solid) and errors (e).

3.5 Spatial and Seasonal patterns of trophic states: Five lake limnetic regions

Previous studies have demonstrated that some lakes disappeared or increased numbers recently according to statistics from Ma et al. (2011). Thus, we selected some representative and stable lakes (*N*=555) to qualify spatial trophic states using the XGBoost algorithm. The preprocessing of MSI data were referred to the Fig.2, and a total of 139 cloud-free images in spring (Apr. and May.), summer (Jul. and Aug.) and autumn (Sep. and Oct.) covered investigated lakes were acquired. According to the different geographic and limnological types in China, lakes were divided into five limnetic regions (Wang and Dou 1998, Early National Investigation): Eastern Plain Limnetic Region (EPLR, *N*=123), Northeast Plain Limnetic Region (NPLR, *N*=37), Inner Mongolia-Xinjiang Plateau Limnetic Region (IMXPLR, *N*=56), Yungui Plateau Limnetic Region (YGPLR, *N*=15), and Tibet-Qinghai Plateau Limnetic Region (TQPLR, *N*=324) (Fig. 1 and Supplementary data).

In general, there were significant seasonal variations in eutrophic state for lakes from the EPLR ($F=39.56$, $p<0.001$) and TQPLR ($F=5.0$, $p<0.05$) (Fig. 7). The averaged *TSI* in EPLR were 56.37 (Spring), 57.73(summer) and 54.26 (autumn) indicating serious eutrophication of investigated lakes, consistent with the results from Li et al., (2022). Recognizing that over 94% of the Chinese population lives in eastern watersheds with great demands of water use, this may be due to different water qualities management in provincial scales. Likewise, we found there was spatial heterogeneity of *TSI* results in TQPLR and some of which were the widespread saline lakes in Qinghai-Tibet Plateau with high reflectance in satellite images. On the contrary, there were no seasonal differences of *TSI* for lakes from IMXPLR, NPLR and YPLR, respectively. The eutrophic lakes dominated the proportions of the investigated lakes in the EPLR (93.5 %), followed by the NPLR (89.2 %), YGPLR (86.7 %), IMXPLR (69.6%) and TQPLR (3.7%) (Fig.8). It can be also found that mesotrophic lakes were found in the decreased order of TQPLR (45.7 %), IMXPLR (30.4%), YGPLR (13.3 %), NPLR (10.8 %) and EPLR (6.5 %), respectively. In comparison, most oligotrophic lakes (50.6%) were distributed in the TQPLR.

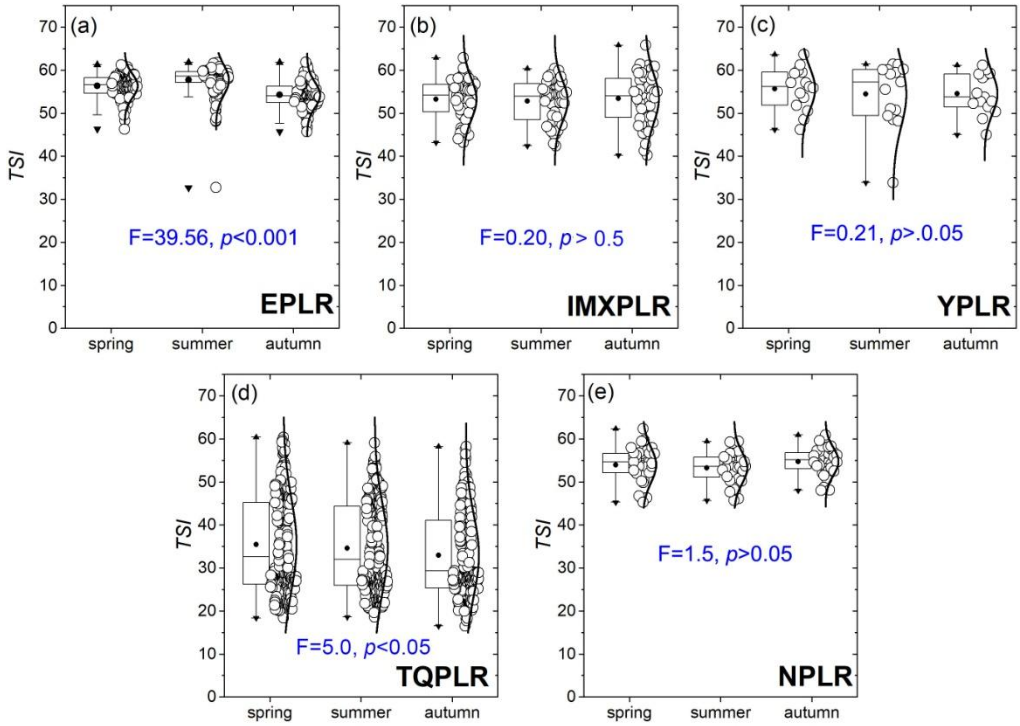

Figure 7 : Box plots of *TSI* derived from XGBoost model in investigated lakes from the five limnetic regions (Wang & Dou 1998), i.e., (a) EPLR, (b) IMXPLR, (c) YPLR, (d) TQPLR and (e) NPLR. The black line and balls in the boxes represent the median and mean values, respectively. The horizontal edges of the boxes denote the 25th and 75th percentiles; the whiskers denote the 10th and 90th percentiles.

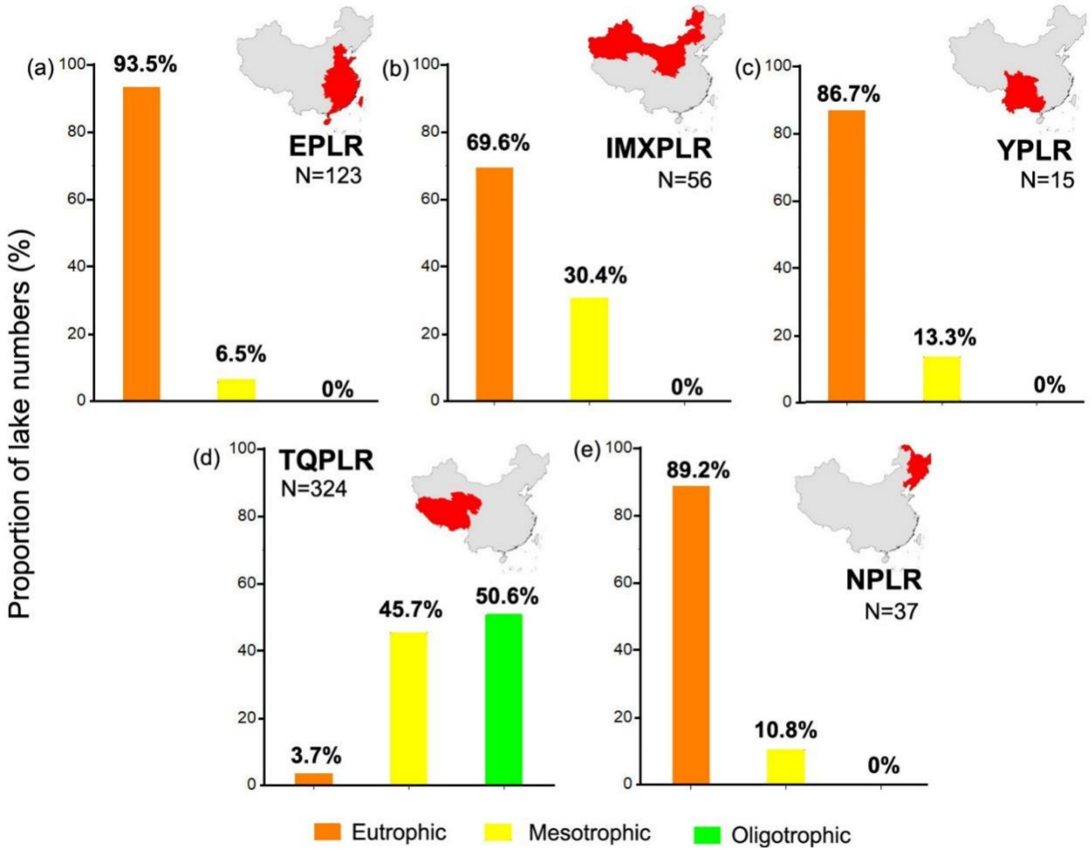

Figure 8: The proportions of lake numbers (%) for different trophic state in the five limnetic regions (Wang & Dou 1998), i.e., (a) EPLR, (b) IMXPLR, (c) YPLR, (d) TQPLR and (e) NPLR. N represents the lake numbers.

4 Discussion

4.1 Remote-sensed and machine-learning-based *TSI* model

Traditional approaches to quantitatively characterize the trophic status rely on field measurements of trophic parameters, for example, Chl-a, nutrients, and SDD, to calculate the *TSI* (Carlson, 1977). It is difficult and costly to make field measurements in lakes in remote locations. The *TSI* calculation does not need all of these trophic parameters but just one, for example, Chl-a (Thiemann and Kaufmann, 2000), SDD (Olmanson et al., 2008; Song et al., 2020), TP (Kutser et al., 1995) and total absorption coefficients (Lee et al., 1999; Shi et al., 2019), etc. There have been many lake studies (Chl-a and SDD, Sheela et al., 2011; Chl-a, SDD and TP, Song et al., 2012) where two or three water quality parameters were mapped, which would allow to subsequently gather them to calculate comprehensive *TSI*. Although these studies provided the potential to evaluate the trophic status of lakes, *TSI* is a synthetic indicator that is affected by biological, physical, and chemical factors that co-vary in most instances. Huang et al. (2014) also tried to derive *TSI* using remote sensing spectrum reflectance, but the accuracy was not completely usable. It shows that variability in remote sensing estimates of the *TSI* are not bad.

With advances in artificial intelligence technology and the increasing use of computer applications in recent years, machine learning has become a useful tool for monitoring aquatic environments by remote sensing (Mountrakis et al., 2011). It allows us to develop and evaluate a machine-learning-based *TSI* model that addresses quality and accuracy problems more effectively (Li et al., 2021). Hence, we propose a new approach to directly characterize the trophic status and accurately reflect spatial variations in this study, but should also be conveniently available for the different lake classifications (Figs. 5, 6). Using machine learning algorithms, in order to improve the robustness and applicability of the *TSI* model, a sufficient database of trophic state parameters (*N*=431) was collected from lakes with different biogeochemical characteristics, such as water quality, absorption contributions of different optically active substances, and reflectance spectra (Table1). We first used B1-B6 reflectance as input variables of machine learning algorithms, and XGBoost showed a significant performance with R^2 and a slope of 0.85 (Fig. S1). The SVM performed worse than XGBoost and random forest, and did not produce the sufficient performance. This is because the latter model are integrated algorithms with trees are unpruned and diverse, signifying the high resolution in the feature space and smoother decision boundary. There was no optical response bands or appropriate band ratios for *TSI*. We thus used a multiple linear regression to find some suitable sensitive band combinations responding to the *TSI*, which made it possible to develop a robust machine-learning-based *TSI* model. It is important to note that the blue/red [*Rrs*(443)/*Rrs*(740), *Rrs*(492)/*Rrs*(740)], and green/red [*Rrs*(560)/*Rrs*(704), *Rrs*(665)/*Rrs*(704)] band ratios were significantly correlated with *TSI* (Table 2). This result indicated that the blue/red and green/red band ratios were more sensitive to the *TSI*, although the nutrients and SDD had no optical response. It was known for decades that the blue part of spectrum is useless when water itself is not blue (i.e. outside of ocean or very oligotrophic mountain lakes), owing to the noneffective atmospheric correction and complex reflectance signals. However, our dataset to train *TSI* models contain the samples from blue and oligotrophic Tibetan lakes, which are like the oceanic environments (Liu et al., 2021). The blue bands responding to *TSI* were thus used in this study. Most empirical Chl-a estimation studies adopted red/near infrared (NIR) band ratios to calibrate models using reflectance signatures (Gitelson et al., 1992). Similarly, empirical SDD retrieval models provided by previous studies used empirical algorithms or models to figure out what bands should work the best considered the following ratios: blue/green, red/blue plus red/green, and red/blue plus blue (Bindling et al., 2007), and Red/Blue ratio plus Blue (Kloiber et al., 2002). Kutser et al. (1995) also built a TP retrieval model using the red and NIR ratios, which is consistent with Chl-a empirical models. Overall, it is not surprising for our *TSI* model to have strong correlations with the blue/red and green/red band ratios because the *TSI* incorporates the optical properties.

For this reason, we used MSI bands in the visible band ratios at six bands, considering the comprehensive spectrum information about the trophic status of lakes as input variables (Fig. 2). The three representative machine learning *TSI* models improved the accuracy of the traditional linear regression (Table 2 and Fig. 5), and the results were better than those obtained with B1-B6 reflectances as input variables (Fig. S1). As a type of supervised machine learning algorithm, linear regression can be used to obtain certain learning criteria as expressions ($y=w_0+w_1\times x_1+\ldots+w_p\times x_p$) about the optimal w_i solution. However, for complex targeted tasks, the fitting ability of linear regression is limited, and it cannot represent the real situation well. For example, a support vector machine can map data to another space, which can use a linear regression to distinguish the categories well. In complex environments (real world in machine learning), such as our large-scale database collected from different lakes (Fig. 1), there are various environmental factors as well as different seasons within a lake, that have an impact on the trophic parameters and optical characteristics of lakes (Wen et al., 2016). Likewise, we found that the enhanced input variables, like the band ratios, if appropriately corrected for the *TSI*, resulted in a better performance (Fig. S1). This is consistent with some applications of machine learning algorithms (Cao et al., 2020), in which the performance of machine learning was reduced when covariances of input features were incorporated. This allows us to find more interesting *TSI*-correlated band ratios for MSI imagery in machine learning.

Several machine learning algorithms generally have different advantages and applicability owing to their different main principles (Cao et al., 2020; Li et al., 2021). This can be found in our results of the validation exercise, which showed that XGBoost provided stable *TSI* estimates, with a slope close to 1 and a good fitting coefficient of the measured and derived values (R^2=0.87, slope=0.85, MAE= 3.15, RMSE=4.11) (Fig. 4). Similarly, we can also find an excellent performance (R^2=0.85, slope=0.84, MAE=3.31, RMSE=4.34) for estimating *TSI* values by the random forest algorithm. This was likely because it is a summation of all weak learners, weighted by the native log odds of error. In the case of boosting, we make decision trees into weak learners by allowing every tree to make only one decision before prediction (Chen et al., 2016). In some cases, XGBoost outperformed random forest. In addition, the support vector machine performed worse than XGBoost and random forest (Fig. 4). Li et al. (2021) used a support vector machine to estimate Chl-a concentrations with a relatively small dataset of 32 samples and 273 samples, respectively. This is consistent with the recent process in the development of support vector machines and has many advantages for remote sensing applications with a small number of training datasets. Overall, the remote sensing and machine learning-based *TSI* model aims to reduce the dependence of traditional field measurements, while also providing a cost-effective approach to rapidly quantify the trophic state.

4.2 *TSI* model for lake classifications

We validated the XGBoost *TSI* model considering different scenarios of lake classification, for example, water quality, optical absorption contributions, and reflectance spectra (Figs. 2 and 6). The results indicate three application scenarios for our model with low errors. The first one is of the XGBoost *TSI* model, which in particular, performed well (slope>0.91, R^2>0.91) in high DOC (>3.88 mg L^{-1}) and EC (>1000 μS cm^{-1}) lakes (Fig. 6). We found that lakes with high EC level correspondingly showed a high DOC level (Table 1), for example, high average EC value of 5156.02 μS cm^{-1} and high average DOC value of 18.75 mg L^{-1} for NAP-type lakes. These brackish or saline lakes were distributed in the Tibet-Qinghai Plateau Region (e.g., KLK20, TS21, QHH22, SLC32, BMC34, ZRNMC36, NMC37) and Inner Mongolia-Xinjiang Plateau Limnetic Region (e.g., DL8, HSH10, DH17, HL18, WLSH16) (Table S1). Our results are in agreement with those of previous studies that DOC and EC of inland waters located in semi-arid region can be attributed to the evapo-concentration and accumulation processes (Curtis and Adams, 1995) as well as anthropogenic activities. Further, it can be observed that oligotrophic lakes accounting for 11.1% were also distributed in the Tibet-Qinghai (Fig. 4).

Secondly, we found that our XGBoost *TSI* model performed well if the trophic parameters that correlated to the TSI_M(Chl-a) or TSI_M(SDD) dominated the lake classifications. Specifically, the high Chl-a (averaged 14.26 μg L^{-1}) and $a_{ph}(440)$ (averaged 0.26 m^{-1}) levels in NAP-type lakes showed the best performance (slope=0.98, R^2=0.88) than those of other optical absorption contribution classifications (Fig. 6). In fact, there was a negligible difference in the performance for application in Phy-type and NAP-type lakes. For the third scenario, for the reflectance spectra classification, cluster-1 lakes with low TSM (averaged 5.76 mg L^{-1}), turbidity (averaged 4.46 NTU), and $a_d(440)$ (averaged 0.26 m^{-1}) level, and high SDD level (average 2.38 m) also showed good performance (slope=0.91, R^2=0.87) (Fig. 6). In general, *TSI*, as a comprehensive index incorporating the optical properties of itself, was calculated using trophic state parameters [(TSI_M(Chl-a), (TSI_M(SDD), and TSI_M(TP) in Eq. 7]. Our XGBoost *TSI* model performed best in the present study, which confirmed that the performance was mostly determined by biogeochemical environments in larger-scale regions. We cannot explain the dependence of the *TSI* model on the physico-optical properties. From another point of view, it can be inferred that the XGBoost *TSI* model applications mostly correlated to the Chl-a and SDD because of their high weight allocation in *TSI* equation.

Although we conducted a large-scale *TSI* observation across Chinese lakes, and if the XGBoost could also perform well for signal lake is required to evaluate. Hence, the *in situ* measured samples were classified in three scenarios, with XGBoost *TSI* model was analyzed. Overall, in future work, for lakes mainly located in high elevation and arid region with high DOC/EC levels, the input band combinations responding to color dissolved organic matter (CDOM, Green/Red) could be added in XGBoost *TSI* model.

This is because that CDOM and DOC generally showed positive correlations for investigated lakes (Song et al., 2013), and CDOM is one of optical active substance. It also confirmed that non-algal particles could cover the reflectance signals and impact on the model performance in second and third scenarios. More classifications based on reflectance spectra (Spyrakos et al., 2018) and water color index (Wang et al., 2018) should be first used and then developed corresponding models for high turbid lakes.

4.3 Trophic status in five limnetic regions

According to this study more than 50% of lakes were eutrophic, indicating a long-standing status of eutrophication (Fig. 4), as seen by the mapping of 555 lakes by our XGBoost *TSI* model (Fig. 7). Some lake investigations undertaken earlier in China during 1978–1980 concluded that 41.2% lakes of eutrophication in China (Jin, 2003), during 1988-1992 demonstrated that 51.2% lakes (Wang & Dou, 1998), during 2001-2005 indicated that 84.5% lakes, during 2011-2019 showed that 50% lakes (Wen et al., 2019) were eutrophic or undergoing eutrophication. In our study, some historical records of Chl-a, SDD and TP from in comparison to earlier national investigation by Wang and Dou (1998) were collected in typical lakes, e.g., Dongting Lake, Poyang Lake, Chaohu Lake, Taihu Lake and Jingpo Lake, respectively (Table S6). Evidently, Chinese lakes have deteriorated considerably in terms of water quality at an alarming rate for typical lakes, e.g., Jingpo Lake, Dongting Lake and Poyang Lake, during past ~22 years (Table S6). Lake eutrophication is influenced by both natural (hydrological processes, topography, lake depth, and buffer capacity) factors as well as anthropogenic factors (land-use changes, urbanization construction, and domestic and industrial pollution) (Müller et al., 1998). A large-scale overview of lake eutrophication indicated there was a significant difference (ANOVA, F=255.2, p<0.001) in the five limnetic regions (Wang & Dou 1998). Owing to the imbalanced development of economic (Fig.S2, GDP and population), geological topography (Fig.S3, solar radiation intensity and sunshine hours) and climate (Fig.S4, annual temperature and precipitation), it was not surprising that the eutrophic lakes were generally distributed in the Eastern Plain Limnetic Region and Northeast Plain Limnetic Region, as well as that the oligotrophic lakes were found in the Tibet-Qinghai Plateau Limnetic Region (Fig.4 and Fig.7).

Considering the natural factors for the distributions of Chinese lake eutrophication, we could suppose some possibility that lake depth and lake hydrological processes cause the eutrophication of lakes in China. Previous studies (Wang & Dou 1998; Huang et al., 2014) have demonstrated that lakes with mean depths > 5 m in China are mainly located in the Yungui Plateau Limnetic Region, Inner Mongolia-Xinjiang Plateau Limnetic Region, and Tibet-Qinghai Plateau Limnetic Region, whereas almost all lakes located in the Eastern Plain Limnetic Region are shallow. Both these lakes in the Eastern Plain Limnetic Region are hydraulically connected with the Yangtze River with a temporary residence time of approximately 30 days (Fig. S7). In shallow lakes, due to wind waves or disturbance by fishes, the phosphorus/nitrogen nutrients stored in the sediment can be easily resuspended and released into the overlying water (Niemistö et al., 2008). Consequently, an increased frequency of algal blooms can be found in Eastern Plain Limnetic Region, in lakes, such as Taihu, Chaohu, and Hongze (Qin et al., 2019; Yao et al., 2016). Instead, deeper lakes, such as the ones in YGPLR and TQPLR, possess relatively good buffer capacity for waste-water runoff (Huang et al., 2014). Carvalho et al. (2009) found that Chl-a levels decreased with lake water depth and geographic location. Qin et al., (2020) and Tong et al., (2006) demonstrated that phosphorus reduction can mitigate eutrophication in deep lakes, and more efforts to reduce both N and P need to be undertaken in shallow lakes. This can be demonstrated in our case of Fuxian Lake with changeable eutrophication levels, with an average depth of 87 m, which was the deepest lake in southwest China (Fig. S7). In addition, the annual precipitation and air temperatures were relatively high in the EPLR (Fig. S4). Hydrological and meteorological processes can scour land surfaces and bring nutrients into lakes via rivers. Therefore, lake ecosystems were strongly related to the lake basin morphology and its hydrologic characteristics, which were higher in shallow lakes than in deep ones (Kõiv et al., 2011).

On the other hand, human-induced eutrophication, for example, agricultural fertilization (Carpenter, 2008; Huang et al., 2017), aquaculture (Guo & Li, 2003) and sewage discharge (Paerl et al., 2011), are increasing terrestrial nutrient phosphorus but not nitrogen concentration inputs (Schindler et al., 2008). We suspected that two interactive factors, such as land-use and nutrient variations cause lake eutrophication, because this can be found in our investigation of distributed lakes in the EPLR in comparison to earlier national investigation by Wang and Dou (1998). Many lakes in the EPLR that were naturally connected with rivers have been modified to paddy fields, and some small lakes have become isolated for lake aquaculture. For instance, Lake Dongting was artificially shifted from being river-fed to dammed/isolated. Logically it should a dam can settle down the suspended matter and nutrients via river inputs. But the shallow characteristic and wind mixing influence process significantly increased the probability of eutrophication (Liu et al., 2019). In EPLR and NPLR, 94% of China's population lives in 43% of its eastern region, which visually demonstrates the distribution of GDP with a densely populated east (Fig. S2). Owing to the requirements of water source utilization, the EPLR has lost one-third of its original lake areas to cropland since 1949 (Yin and Li, 2001). Lake aquaculture is highly active in these areas. These processes could lead to terrestrial nutrient loading into lakes, from either agriculture or aquaculture, and thereby alter the trophic state levels of a lake ecosystem. In 2019, the total fish catch in Hubei was 4,695 tons; in Jiangxi was 432, 25 tons; in Anhui was 588,135 tons; 2,314,603 and 4,841,159 tons in Anhui and Jiangsu in the east, respectively (China rural statistical yearbook).

Although we have not systematically analyzed the effects of environmental factors on trophic status, some of the sparse existing comparative literature supported certain spatiotemporal patterns. It should be emphasized that China has been facing serious lake eutrophication and unbalanced distributions. Almost invariably, lake ecosystem health would still be impacted by stresses integrating anthropogenic and overexploitation of catchment resources. Consequently, addressing the issue of worsening eutrophication requires a better understanding of the environmental interactive mechanisms in the future.

4.4 Limitations, uncertainties and future

Toward the United Nation's Sustainable Development Goal (SDG) 6.3.2, satellite imagery and machine learning still provides great potential for evaluating water qualities state from global observations, particularly in developing countries. Machine learning algorithms could serve as good alternatives for empirical and semi-analytical algorithms to quantify on large-scale spatial applications, which could avoid or minimize the errors.Our results further demonstrated machine learning algorithms could improve the accuracy of water quality models (e.g., *TSI*) when the linear regression was used to find sensitive band combinations with red/red edge bands. Previous studies (Li et al., 2021, 2022) found red and red edge band could help us to quantify the spatial and temporal changes of Chl-a concentration or a synthetic parameter-such as *TSI* with high Chl-a weight ratio-from regional lakes. It is enable us to use sentinel-2 or similar sensors equipped with these bands to capture records of *TSI* dynamics.

As a medium-resolution (10~60 m) satellite, Sentinel-2 MSI offers the potential to monitor small-size lakes and produce reliable *TSI* estimates. However, there are significant obstacles in generating a Sentinel-2 (~10m) lake *TSI* distribution, including the acquisition of high quality atmospheric corrected Rrs(λ) and massive computational overhead by C2RCC processor (Li et al., 2023). C2RCC processor designed for waters based on neural networks is data-driven approach and uses huge datasets collected from *in situ* and simulation measurements. *In situ* reflectance measurements were not conducted in these investigated Chinese lakes when sampling. Our recently study reported that C2RCC (SNAP 8.0) and Polymer (v4.13) processors both performed best with *in situ* field radiometry in typical lakes across China (Li et al., 2023), but the latter could work better when all bands are pooled together in derived algorithms. Considering the growing requirements of *TSI* products, more *in situ* measurements would be required to be added the already-implemented processors in following work.

In addition, there is a need for a robust model developed from different locations and optical water types that accounts for the interplay of different water quality parameters. Machine learning *TSI* model required a highly calibrated dataset, including high nutrients (e.g., TP >2.50 mg L^{-1} in this study) and Chl-a concentrations (>100 μg L^{-1} in this study). Likewise, for our developed universal *TSI* model, the feasibility application performances were different considering lake classifications. Hence, the extensive field–lab materials with complex source variations would be required first and water optical typologies further is a good compromise to develop groups of optimized algorithms in future. Nevertheless, we aim to provide technical operation approach, which could prompt more analysis responding to warming climate and anthropogenic activities. The strong linkages between reflectance and several trophic state defining indexes further underscore the potential of remote sensing for resources-limited countries meet their SDG goals.

5 Conclusions

Our study presents a novel remote sensing- and machine-learning-based algorithm applied in that allow to retrieve the lake *TSI* from Sentinel-2 MSI imagery. We used a match-up database (*N*=431) over a diverse range of bio-optical regimes to train machine learning algorithms and validated it against the in situ data. The trophic states of 555 lakes were then evaluated. These results provide a better understanding how remote sensing and machine learning-based models allow to estimate eutrophication over a large scale of different lakes. Our main findings can be summarized as follows:

1) Linear regression enabled us to find certain band combinations sensitive to *TSI* (R^2>0.59), for example, the blue/red [*Rrs*(443)/*Rrs*(740), *Rrs*(492)/*Rrs*(740)] and green/red [*Rrs*(560)/*Rrs*(704), *Rrs*(665)/*Rrs*(704)] band ratios.

2) XGBoost algorithm resulted in optimum performance with R^2=0.87 and slope=0.85, considering the low errors (MAE=3.15, RMSE=4.11), compared to the support vector machine and random forest algorithms.

3) If there is some preliminary data available from the study area one can improve the performance of the machine learning by dividing the lakes based on high DOC/EC, NAP-type and Phy-type, and cluster-1 reflectance spectra.

4) The trophic states of 555 lakes were evaluated in five limnetic regions; eutrophic lakes dominated in Eastern Plain Limnetic Region and Northeast Plain Limnetic Region, and most lakes in Tibet-Qinghai Plateau Limnetic Region were mesotrophic or oligotrophic.

In our subsequent research and management, qualification and mapping of *TSI* will be implemented as a remote sensing and machine learning model in a large-scale study, allowing for an improved performance. In the future, Sentinel-2 MSI data could be used to reveal spatiotemporal variations in lake trophic states in long-term time-series responding to climate and anthropogenic activities.

Data availability. The data used in this study are openly available for research purposes. The MSI imagery was acquired from Copernicus Open Access Hub of the European Space Agency (https://scihub.copernicus.eu).The SNAP software is available at https: //step.esaint/main/download/snap-download.

Author contributions. Sijia Li: Conceptualization, Methodology, Formal analysis, Visualization, Funding acquisition, Writing original draft. Kaishan Song: Resources, Supervision, Project administration, Funding acquisition, Writing-review & editing. Tiit Kuster: Writing-review & editing. Ge Liu: Resources, Writing-review & editing. Shiqi Xu: Methodology. Zhidan Wen: Resources, Writing-review & editing. Yingxin Shang: Resources, Writing-review & editing. Lili Lyu: Investigation & Resources. Hui Tao: Investigation & Resources.

Competing interests. The contact author has declared that none of the authors has any competing interests.

Disclaimer. Publisher's note: Copernicus Publications remains neutral with regard to jurisdictional claims in published maps and institutional affiliations

Acknowledgements. The authors thank all staff and students of IGACAS for their persistent assistance with both field sampling and laboratory analysis. The authors express their gratitude to the four anonymous reviewers for their constructive comments and suggestions that have helped improve the paper.

Financial support. The research was jointly supported by the National Natural Science Foundation of China (U2243230, 42201414, 42171374, 42071336, 42171385, 42101366 and 42001311) and Land Observation Satellite Supporting Platform of National Civil Space Infrastructure Project (CASPLOS-CCSI).

References

APHA, A. W., Standard Methods for the examination of water and wastewater 20th edition.,https://doi.org/10.2105/AJPH.51.6.940-a,1961.

American Public Health Association/American Water Works Association/Water Environment Federation, Washington DC, USA,https://doi.org/10.1080/23267224.1919.10651076,1998.

Aizaki, M., Otsuki, A., Fukushima, T., et al., Application of Carlson's trophic state index to Japanese lakes and relationships between the index and other parameters: With 2 figures and 4 tables in the text. Internationale Vereinigung für theoretische und angewandte Limnologie: Verhandlungen, 21(1), 675-681.Res.rep.natl.inst.environ.stud.jpn, 1981.

Carpenter, S. R., Brock, W. A., Cole, J. J., et al., Leading indicators of trophic cascades. Ecol. Lett. 11(2), 128-138,https://doi.org/10.1111/j.1461-0248.2007.01131.x,2008.

Carlson, R. E., A trophic state index for lakes 1. Limnol. Oceanogr. 22(2), 361-369.https://doi.org/10.2307/2834910,1977.

Chen, T., Guestrin, C., Xgboost: A scalable tree boosting system. In *Proceedings of the 22nd acm sigkdd international conference on knowledge discovery and data mining* (pp. 785-794).

Cleveland, J. S., Weidemann, A. D., Quantifying absorption by aquatic particles: A multiple scattering correction for glass-fiber filters. Limnol. Oceanogr. 38(6), 1321-1327, https://doi.org/10.4319/lo.1993.38.6.1321,1993.

Cunha, D. G. F., do Carmo Calijuri, M., Lamparelli, M. C., A trophic state index for tropical/subtropical reservoirs (TSItsr). Ecol. Eng. 60, 126-134. https://doi.org/10.1016/j.ecoleng.2013.07.058,2013.

Curtis, P. J., Adams, H. E., Dissolved organic matter quantity and quality from freshwater and saltwater lakes in east-central Alberta. Biogeochemistry 30(1), 59-76. https://doi.org/10.1007/bf02181040,1995.

Doerffer, R., Schiller, H., The MERIS Case 2 water algorithm. Int. J Remote sens. 28(3-4), 517-535. https://doi.org/10.1080/01431160600821127,2007.

Duarte, C. M., Prairie, Y. T., Montes, C., et al., CO2 emissions from saline lakes: A global estimate of a surprisingly large flux. J. Geophys. Res.-Biogeosciences 113(G4). https://doi.org/10.1029/2007jg000637,2008.

Drusch, M., Del Bello, U., Carlier, S., et al., Sentinel-2: ESA's optical high-resolution mission for GMES operational services. Remote Sens. Environ.120, 25-36, https://doi.org/10.1109/igarss.2007.4423394,2012.

Fragoso Jr, C. R., Marques, D. M. M., Ferreira, T. F., et al., 2011. Potential effects of climate change and eutrophication on a large subtropical shallow lake. Environ. Modell. Softw. 26(11), 1337-1348, https://doi.org/10.1016/j.envsoft.2011.05.004,2011.

Gitelson, A.The peak near 700 nm on radiance spectra of algae and water: relationships of its magnitude and position with chlorophyll concentration. International Journal of Remote Sensing, 13(17), 3367-3373, https://doi.org/10.1080/01431169208904125,1992.

Gitelson, A. A., Dall'Olmo, G., Moses, W., et al., 2008. A simple semi-analytical model for remote estimation of chlorophyll-a in turbid waters: Validation. Remote Sens. Environ. 112(9), 3582-3593. https://doi.org/10.1080/01431169208904125,1992.

Gurlin, D., Gitelson, A. A., Moses, W. J., Remote estimation of chl-a concentration in turbid productive waters—Return to a simple two-band NIR-red model?. Remote Sens. Environ. 115(12), 3479-3490. https://doi.org/10.1016/j.rse.2011.08.011,2011.

Guo, L., Li, Z., Effects of nitrogen and phosphorus from fish cage-culture on the communities of a shallow lake in middle Yangtze River basin of China. Aquaculture 226(1-4), 201-212. https://doi.org/10.1016/S0044-8486(03)00478-2,2003.

Guo, M., Li, X., Song, C., et al., Photo-induced phosphate release during sediment resuspension in shallow lakes: A potential positive feedback mechanism of eutrophication. Environ Pollut. 258, https://doi.org/113679. 10.1016/j.envpol.2019.113679

Huang, C., Wang, X., Yang, H., et al., Satellite data regarding the eutrophication response to human activities in the plateau lake Dianchi in China from 1974 to 2009. Sci. Total Environ. 485, 1-11. https://doi.org/10.1016/j.scitotenv.2014.03.031,2014.

Huang, J., Xu, C. C., Ridoutt, B. G., et al., Nitrogen and phosphorus losses and eutrophication potential associated with fertilizer application to cropland in China. J. Clean. Prod. 159, 171-179. https://doi.org/10.1016/j.jclepro.2017.05.008,2017.

Hu, M., Zhang, Y., Ma, R., et al., Optimized remote sensing estimation of the lake algal biomass by considering the vertically heterogeneous chlorophyll distribution: Study case in Lake Chaohu of China. Sci. Total Environ. 771, 144811. https://doi.org/10.1016/j.scitotenv.2020.144811,2021.

ILEC/Lake Biwa Research Institute 1994 1988-1993 survey of the state of the world's lakes Volumes I-IV (International Lake Environment Committee, Otsu and United Nations Environment Programme: Nairobi, Kenya)

Jeffrey, S. T., Humphrey, G. F., New spectrophotometric equations for determining chlorophylls a, b, c1 and c2 in higher plants, algae and natural phytoplankton. Biochemie und physiologie der pflanzen 167(2), 191-194. https://doi.org/10.1016/0022-2860(75)85046-0,1975.

Jin, X., Hu, X., A comprehensive plan for treating the major polluted regions of Lake Taihu, China. Lakes & Reservoirs: Research & Management 8(3-4), 217-230. https://doi.org/10.1111/j.1440-1770.2003.00220.x,2003.

Jin, X., Xu, Q., Huang, C., Current status and future tendency of lake eutrophication in China.

Science in China Series C: Life Sciences 48(2), 948-954.https://doi.org/10.1007/BF03187133,2005.

Kloiber, S. M., Brezonik, P. L., Olmanson, L. G., et al., A procedure for regional lake water clarity assessment using Landsat multispectral data. Remote Sens. Environ. 82(1), 38-47. https://doi.org/10.1016/S0034-4257(02)00022-6,2002.

Koiv, T., Nõges, T., Laas, A., Phosphorus retention as a function of external loading, hydraulic turnover time, area and relative depth in 54 lakes and reservoirs. Hydrobiologia 660(1), 105-115. https://doi.org/10.1007/s10750-010-0411-8,2011.

Li, S., Song, K., Wang, S., et al., Quantification of chlorophyll-a in typical lakes across China using Sentinel-2 MSI imagery with machine learning algorithm. Sci. Total Environ. 778, 146271. https://doi.org/10.1016/j.scitotenv.2021.146271,2021.

Liu, D., Duan, H., Yu, S., et al., 2019. Human-induced eutrophication dominates the bio-optical compositions of suspended particles in shallow lakes: Implications for remote sensing. Sci. Total Environ. 667, 112-123. https://doi.org/10.1016/j.scitotenv.2019.02.366

Lund, J. W., Eutrophication. Nature 214(5088), 557-558.https://doi.org/10.1038/214557a0,1967.

Ma, Y. L., Zhang, W. B., Yu, B., et al., Prevalence of allergic bronchopulmonary aspergillosis in Chinese patients with bronchial asthma. Zhonghua jie he he hu xi za zhi= Zhonghua jiehe he huxi zazhi= Chinese journal of tuberculosis and respiratory diseases, 34(12), 909-913.

https://doi.org/10.1038/cmi.2011.4,2011.

Matthews, M. W., Eutrophication and cyanobacterial blooms in South African inland waters: 10 years of MERIS observations. Remote Sens. Environ. 155, 161-177. https://doi.org/10.1016/j.rse.2010.04.013,2014.

Matthews, M. W., Odermatt, D., Improved algorithm for routine monitoring of cyanobacteria and eutrophication in inland and near-coastal waters. Remote Sens. Environ. 156, 374-382. https://doi.org/10.1016/j.rse.2014.10.010,2015.

Mortsch, L. D., Quinn, F. H.,Climate change scenarios for Great Lakes Basin ecosystem studies. Limnol. Oceanogr. 41(5), 903-911.https://doi.org/10.4319/lo.1996.41.5.0903,1996.

Morel, A., Prieur, L., 1977. Analysis of variations in ocean color 1. Limnol. Oceanogr. 22(4), 709-722.

Müller, B., Lotter, A. F., Sturm, M., et al., Influence of catchment quality and altitude on the water and sediment composition of 68 small lakes in Central Europe. Aquat. Sci. 60(4), 316-337. https://doi.org/10.1007/s000270050044,1998.

Mountrakis, G., Im, J., Ogole, C.,Support vector machines in remote sensing: A review. ISPRS-J. Photogramm. Remote Sens. 66(3), 247-259.https://doi.org/10.1016/j.isprsjprs.2010.11.001,2011.

Neil, C., Spyrakos, E., Hunter, P. D., et al., A global approach for chlorophyll-a retrieval across optically complex inland waters based on optical water types. Remote Sens. Environ. 229, 159-178. https://doi.org/10.1016/j.rse.2019.04.027,2019.

Niemistö, J., Holmroos, H., Pekcan-Hekim, Z., et al., Interactions between sediment resuspension and sediment quality decrease the TN: TP ratio in a shallow lake. Limnol. Oceanogr. 53(6), 2407-2415. https://doi.org/10.2307/40058331,2008.

OECD (Organization for Economic Cooperation and Development). 1982. Eutrophication of waters: monitoring, assessment and control. Organisation for Economic and Cooperative Development, Paris, France.

Oliver, S. K., Collins, S. M., Soranno, P. A., et al.,Unexpected stasis in a changing world: Lake nutrient and chlorophyll trends since 1990. Glob. Change Biol. 23(12), 5455-5467 . https://doi.org/10.1111/gcb.13810,2017.

Olmanson, L. G., Bauer, M. E., Brezonik, P. L., A 20-year Landsat water clarity census of Minnesota's 10,000 lakes. Remote Sens. Environ. 112(11), 4086-4097. https://doi.org/10.1111/jawr.12138,2008.

Pan, Q., Dias, D., An efficient reliability method combining adaptive support vector machine and Monte Carlo simulation. Struct. Saf. 67, 85-95.https://doi.org/10.1016/j.strusafe.2017.04.006,2017.

Paerl, H.,Nutrient and other environmental controls of harmful cyanobacterial blooms along the freshwater–marine continuum. In Cyanobacterial harmful algal blooms: State of the science and research needs (pp. 217-237). Springer, New York, NY. https://doi.org/10.1007/978-0-387-75865-7_10,2008.

Paerl, H. W., Xu, H., McCarthy, M. J., et al., Controlling harmful cyanobacterial blooms in a hyper-eutrophic lake (Lake Taihu, China): the need for a dual nutrient (N & P) management strategy. Water Res. 45(5), 1973-1983. https://doi.org/10.1016/j.waters.2010.09.018,2011.

Pahlevan, N., Chittimalli, S. K., Balasubramanian, S. V., et al.,Sentinel-2/Landsat-8 product consistency and implications for monitoring aquatic systems. Remote Sens. Environ. 220, 19-29. https://doi.org/10.1016/j.rse.2018.10.027,2019.

Pahlevan, N., Smith, B., Schalles, J., et al.,Seamless retrievals of chlorophyll-a from Sentinel-2 (MSI) and Sentinel-3 (OLCI) in inland and coastal waters: A machine-learning approach. Remote Sens. Environ. 240, 111604. https://doi.org10.1016/j.rse.2019.111604,2020.

Prieur, L., Sathyendranath, S.,An optical classification of coastal and oceanic waters based on the specific spectral absorption curves of phytoplankton pigments, dissolved organic matter, and other particulate materials 1. Limnol. Oceanogr. 26(4), 671-689. https://doi.org/10.4319/lo.1981.26.4.0671,1981.

Qin, B., Gao, G., Zhu, G., et al., Lake eutrophication and its ecosystem response. Chinese Sci. Bull. 58(9), 961-970. https://doi.org/10.1007/s11434-012-5560-x,2013.

Qin, B., Zhou, J., Elser, J. J., et al.,Water depth underpins the relative roles and fates of nitrogen and phosphorus in lakes. Environ. Sci. Technol. 54(6), 3191-3198. https://doi.org/10.1021/acs.est.9b05858,2020.

Quayle, W. C., Peck, L. S., Peat, H., et al.,Extreme responses to climate change in Antarctic lakes. (Climate Change). Science 295(5555), 645-646.https://doi.org/10.1126/science.1064074,2002.

Reichstein, M., Camps-Valls, G., Stevens, B., et al.,Deep learning and process understanding for data-driven Earth system science. Nature 566(7743), 195-204. https://doi.org/10.1038/s41586-019-0912-1,2019.

Rodhe, W., 1969. Crystallization of eutrophication concepts in northern Europe.

Sass, G. Z., Creed, I. F., Bayley, S. E.et al.,Understanding variation in trophic status of lakes on the Boreal Plain: A 20 year retrospective using Landsat TM imagery. Remote Sens. Environ.109(2), 127-141. https://doi.org/10.1016/j.rse.2006.12.010,2007.

Schindler, D. W., Hecky, R. E., Findlay, D. L., et al.,Eutrophication of lakes cannot be controlled by reducing nitrogen input: results of a 37-year whole-ecosystem experiment. Proceedings of the National Academy of Sciences, 105(32), 11254-11258. https://doi.org/10.1109/ICASSP.2002.5745032,2008.

Sheela, A. M., Letha, J., Joseph, S., et al.,Trophic state index of a lake system using IRS (P6-LISS III) satellite imagery. Environ. Monit. Assess. 177(1), 575-592.

https://doi.org/10.1007/s10661-010-1658-2,2011.

Shi, K., Zhang, Y., Song, K., et al., 2019. A semi-analytical approach for remote sensing of trophic state in inland waters: Bio-optical mechanism and application. Remote Sens. Environ. 232, 111349.

Smith, V. H., Tilman, G. D., Nekola, J. C.,Eutrophication: impacts of excess nutrient inputs on freshwater, marine, and terrestrial ecosystems. Environ. Pollut. 100(1-3), 179-196. https://doi.org/10.1016/j.rse.2019.111349,1999.

Smith, V. H., Joye, S. B., Howarth, R. W., 2006. Eutrophication of freshwater and marine ecosystems. Limnol. Oceanogr. 51(1part2), 351-355. https://doi.org/10.4319/lo.2006.51.1_part_2.0351,2006.

Smith, V. H., Schindler, D. W.,Eutrophication science: where do we go from here?. Trends Ecol. Evol. NLM. 24(4), 201-207. https://doi.org/10.1016/j.tree.2008.11.009,2009.

Song, K., Li, L., Tedesco, L. P., et al.,Hyperspectral determination of eutrophication for a water supply source via genetic algorithm–partial least squares (GA–PLS) modeling. Sci. Total Environ. 426, 220-232. https://doi.org/10.1016/j.scitotenv.2012.03.058,2012.

Song, K. S., Zang, S. Y., Zhao, Y., et al.,Spatiotemporal characterization of dissolved carbon for inland waters in semi-humid/semi-arid region, China. Hydrol. Earth Syst. Sci. 17(10). https://doi.org/10.5194/hessd-10-6559-2013,2013a.

Song, K., Li, L., Tedesco, L. P., Li, S., 2013b. Remote estimation of chlorophyll-a in turbid inland waters: Three-band model versus GA-PLS model. Remote Sens. Environ. 136, 342-357. https://doi.org/10.1016/j.rse.2013.05.017,2013b.

Song, K., Liu, G., Wang, Q., et al.,Quantification of lake clarity in China using Landsat OLI imagery data. Remote Sens. Environ. 243, 111800. https://doi.org/10.1016/j.rse.2020.111800,2020.

Thiemann, S., Kaufmann, H., 2000. Determination of chlorophyll content and trophic state of lakes using field spectrometer and IRS-1C satellite data in the Mecklenburg Lake District, Germany. Remote Sens. Environ. 73(2), 227-235. https://doi.org/10.1016/S0034-4257(00)00097-3,2000.

Toming, K., Kotta, J., Uuemaa, E., Sobek, S., Kutser, T., & Tranvik, L. J. Predicting lake dissolved organic carbon at a global scale. Scientific reports 10(1), 1-8. https://doi.org/10.1038/s41598-020-65010-3,2020.

Tong, Y., Zhang, W., Wang, X., et al.,Decline in Chinese lake phosphorus concentration accompanied by shift in sources since 2006. *Nature Geoscience*, *10*(7), 507-511. https://doi.org/10.1038/ngeo2967,2017.

Tranvik, L. J., Downing, J. A., Cotner, J. B., et al.,Lakes and reservoirs as regulators of carbon cycling and climate. Limnol. Oceanogr. 54(6part2), 2298-2314. https://doi.org/10.4319/lo.2009.54.6_part_2.2298,2009.

USEPA, A., 2002. National water quality inventory 2000 report. EPA-841-R-02-001.

Wetzel, R. G.,Limnology: lake and river ecosystems. gulf professional publishing. https://doi.org/10.1086/380040,2001.

Wang, S., Li, J., Zhang, B., et al.,Trophic state assessment of global inland waters using a MODIS-derived Forel-Ule index. Remote Sens. Environ. 217, 444-460. https://doi.org/10.1016/j.rse.2018.08.026,2018.

Wang, S. and Hongsheng, D., 1998. Chinese Lake Records, Beijing, Science Publishing (in Chinese).

Warren, M. A., Simis, S. G., Martinez-Vicente, et al.,Assessment of atmospheric correction algorithms for the Sentinel-2A MultiSpectral Imager over coastal and inland waters. Remote Sens. Environ. 225, 267-289. https://doi.org/10.1016/j.rse.2019.03.018,2019.

Wen, Z., Song, K., Liu, G., et al., Quantifying the trophic status of lakes using total light absorption of optically active components. Environ. Pollut. 245, 684-693. https://doi.org/10.1016/j.envpol.2018.11.058,2019.

Wen, Z. D., Song, K. S., Zhao, Y., et al., Influence of environmental factors on spectral characteristics of chromophoric dissolved organic matter (CDOM) in Inner Mongolia Plateau, China. Hydrol Earth Syst sc, 20(2), 787-801. https://doi.org/10.5194/hess-20-787-2016

Wiley, C.,What motivates employees according to over 40 years of motivation surveys. International journal of manpower. https://doi.org/10.1108/01437729710169373,1997.

Wu, G., Xu, Z., Prediction of algal blooming using EFDC model: Case study in the Daoxiang Lake. Ecol Modell. 222(6), 1245-1252. https://doi.org/10.1016/j.ecolmodel.2010.12.021,2011.

Yao, Y., Wang, P., Wang, C., et al., Assessment of mobilization of labile phosphorus and iron across sediment-water interface in a shallow lake (Hongze) based on in situ high-resolution measurement. Environ. Pollut. 219, 873-882. https://doi.org/10.1016/j.envpol.2016.08.054,2016.

Yin, H., Li, C., Human impact on floods and flood disasters on the Yangtze River. Geomorphology 41(2-3), 105-109. https://doi.org/10.1016/S0169-555X(01)00108-8,2001.

Yin, H., Douglas, G. B., Cai, Y., et al., Remediation of internal phosphorus loads with modified clays, influence of fluvial suspended particulate matter and response of the benthic macroinvertebrate community. Sci. Total Environ. 610, 101-110. https://doi.org/10.1016/j.scitotenv.2017.07.243, 2018.

Zhang, Y., Zhou, Y., Shi, K., et al., Optical properties and composition changes in chromophoric dissolved organic matter along trophic gradients: Implications for monitoring and assessing lake eutrophication. Water Res. 131, 255-263. https://doi.org/10.1016/j.watres.2017.12.051,2018.